Low-intensity pulsed ultrasound induces proliferation of human neural stem cells

Al-Maswary, Arwa; Walmsley, Damien; Cooper, Paul; Scheven, Ben

DOI:
10.1002/ctd2.259

Document Version
Publisher's PDF, also known as Version of record

Citation for published version (Harvard):
Al-Maswary, A, Walmsley, D, Cooper, P & Scheven, B 2024, 'Low-intensity pulsed ultrasound induces proliferation of human neural stem cells', *Clinical and Translational Discovery*, vol. 4, no. 2, e259. https://doi.org/10.1002/ctd2.259

Received: 29 September 2023 | Revised: 22 December 2023 | Accepted: 26 December 2023

DOI: 10.1002/ctd2.259

CLINICAL AND TRANSLATIONAL DISCOVERY Open Access WILEY

RESEARCH ARTICLE

Low-intensity pulsed ultrasound induces proliferation of human neural stem cells

Arwa A. Al-Maswary[1] | **A. Damien Walmsley**[1] | **Paul R. Cooper**[1,2] | **Ben A. Scheven**[1]

[1]School of Dentistry, Institute of Clinical Sciences, College of Medical and Dental Sciences, University of Birmingham, Birmingham, UK

[2]Sir John Walsh Research Institute, Faculty of Dentistry, University of Otago, Dunedin, New Zealand

Correspondence
Arwa A. Al-Maswary and Ben A. Scheven, School of Dentistry, Institute of Clinical Sciences, College of Medical and Dental Sciences, University of Birmingham, Birmingham, UK.
Email: AAA680@alumni.bham.ac.uk and b.a.scheven@bham.ac.uk

Graphical Abstract

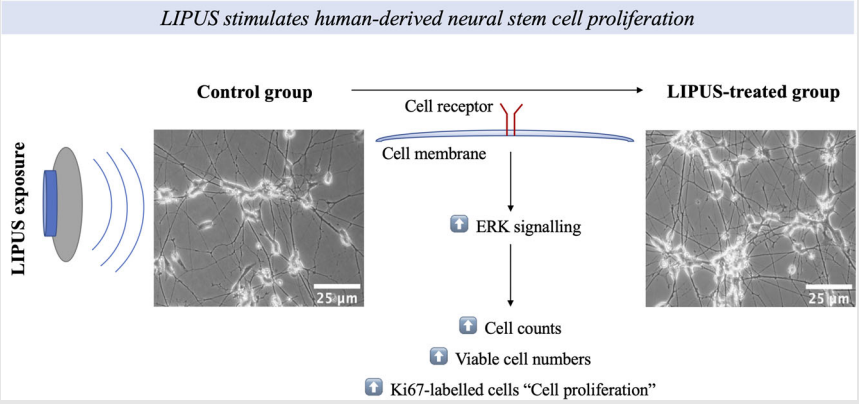

- Low-intensity pulsed ultrasound (LIPUS) stimulates proliferation of SH-SY5Y-derived neural stem cells.
- Single LIPUS exposure produced significant neural stem cell numbers, but triple LIPUS exposures resulted in greater neural stem cell numbers than the single LIPUS exposure, albeit the difference was not statistically significant.
- ERK signalling plays a role in the induction of the cell proliferation induced by LIPUS.

Received: 29 September 2023 | Revised: 22 December 2023 | Accepted: 26 December 2023

DOI: 10.1002/ctd2.259

RESEARCH ARTICLE

CLINICAL AND TRANSLATIONAL DISCOVERY Open Access

WILEY

Low-intensity pulsed ultrasound induces proliferation of human neural stem cells

Arwa A. Al-Maswary[1] | **A. Damien Walmsley**[1] | **Paul R. Cooper**[1,2] | **Ben A. Scheven**[1]

[1]School of Dentistry, Institute of Clinical Sciences, College of Medical and Dental Sciences, University of Birmingham, Birmingham, UK

[2]Sir John Walsh Research Institute, Faculty of Dentistry, University of Otago, Dunedin, New Zealand

Correspondence
Arwa A. Al-Maswary and Ben A. Scheven, School of Dentistry, Institute of Clinical Sciences, College of Medical and Dental Sciences, University of Birmingham, Birmingham, UK.
Email: AAA680@alumni.bham.ac.uk and b.a.scheven@bham.ac.uk

The work was done in the School of Dentistry, University of Birmingham, Birmingham, UK.

Abstract

Background: Low-intensity pulsed ultrasound (LIPUS) has been highlighted as a potential therapy for tissue repair and regeneration. However, little is known about LIPUS effects on neuromodulation. This research was conducted to study LIPUS effect on the proliferation of human neural stem cells.

Materials and methods: The human SH-SY5Y neuroblastoma cell line was used as a neural stem cell model. The well-documented SH-SY5Y neurogenic protocol, which involves treatment with all trans-retinoic acid (ATRA) for 5 days and then brain-derived neurotrophic factor (BDNF) for 7 days, was used to synchronise the growth cell cycle to G1 phase of the cell cycle before proliferation testing. Subsequently, the neural stem cells were then treated with single or triple 20-min LIPUS exposures (Intensity I_{SATA}: 60 mW/cm^2, frequency: 1.5 MHz, pulse repetition: 100 Hz, and duty cycle: 20%). Cell proliferation was analysed using cell counting of β-tubulin and neurofilament medium-positive neural stem cells, Ki67-cell proliferation marker and metabolic-based assays (cell counting kit-8 and alamarBlue). The involvement of ERK signalling was investigated by quantification of phospho-ERK1/2 levels and cell proliferation with and without MEK/ERK inhibitor (U0126).

Results: The results show that LIPUS exposure(s) induced cell proliferation, as evidenced by an increase in the numbers of neural stem cells. ERK signalling is involved in LIPUS-induced neural stem cell proliferation, as evidenced by concurrent inhibition of LIPUS-induced phospho-ERK levels and cell proliferation in the presence of the MEK/ERK inhibitor.

Conclusion: This study provides original evidence that LIPUS can stimulate neural stem/progenitor cell proliferation. LIPUS may be suggested as a sole or an adjunct therapeutic application to promote the neural stem cell pool in stem cell therapies and tissue engineering approaches for nerve repair and regeneration for the management of traumatic nerve injuries and regenerative endodontic treatment.

KEYWORDS
cell proliferation, ERK/MAPK, human, LIPUS, neural stem cells, SH-SY5Y

1 | INTRODUCTION

Low-intensity pulsed ultrasound (LIPUS) has gained interest over recent years as a safe, non-invasive and inexpensive clinical therapeutic tool to promote tissue regeneration and repair.[1,2] LIPUS has been approved as a therapy for delayed fractured bone union by the Food and Drug Administration (FDA).[3] It has been advocated as a therapy for nerve repair and neuromodulation of rat nerve injuries.[4–10] In this context, most LIPUS studies were conducted either on animals 'in vivo'[4–10] or on their cells 'in vitro',[11–15] which cannot fully simulate human cells and genes hindering the translation of therapies to human.[16–19] Furthermore, few studies have described LIPUS effects on human-derived neural stem cells.[5,20,21] Hence, overall, little is known about the LIPUS effects on human neural stem cells.

As a preclinical step, in vitro human neural stem cells are required to investigate such a therapy. As it is prohibited to obtain primary human neural stem cells due to ethical concerns, human-derived neural cell line is an alternative option to study the therapeutic effects.[22,23] In this context, the human-derived SH-SY5Y neuroblastoma cell line[24] is a basic and consistent neural model for neurological testing.[25–27] SH-SY5Y is a subcloned cell line derived from a neuroblastoma of bone marrow in a 4-year-old girl,[24,28] which is widely used in neuroscience such as investigating Parkinson and Alzheimer's diseases,[29,30] neurotoxicity,[31,32] energetic neural vulnerability[33] and being a control model for neurogenic induction of stem cells[34,35] and their neurotrophic effects.[36,37] However, the SH-SY5Y cell cultures lack mature neural features,[33,38,39] and due to neuroblastoma 'cancerous' origin, the cells exhibit high proliferative rate[40] with unsynchronised cell cycles,[22,41] which will negatively affect the reliability and reproducibility of the cell mitosis-related studies such as cell proliferation.[42,43] As the neurogenic induction of the SH-SY5Y cell line increases the neural characteristics and synchronises the cell cycle[22,38,40] with low proliferation rate,[38,44,45] which resembles the primary stem cells,[40] this study was designed to be conducted on neurogenic-induced cells. In this context, the chosen neurogenic protocol using all trans-retinoic acid (ATRA) and brain-derived neurotrophic factors (BDNFs) has been proven to increase neural morphology and biomarkers,[38,39,46] functionality-related genes[47] and electrophysiological profile.[48] Therefore, this study aimed to investigate the proliferative effect of LIPUS on neural stem cells established from SH-SY5Y.

2 | MATERIALS AND METHODS

2.1 | Cell culture and neurogenic preparation

SH-SY5Y neuroblastoma cells (ATCC CRL-2266) were used at passages of 18–22 and cultured in Dulbecco's modified Eagle's medium/mixture F-12 Ham (DMEM/F-12) (Sigma-Aldrich). The DMEM/F-12 was supplemented with 10% foetal bovine serum (FBS) (Biosera) and 1% penicillin-streptomycin (100 I.U./mL) (Sigma-Aldrich). Subsequently, the SH-SY5Y cells were kept in an incubator at 37°C and 5% CO_2 (Heracell 150i, Thermo Scientific). The media changes were performed every 3 days till the cultures reached approximately 80% cell confluence. As the cell cultures exhibit a mixture of adherent (S-type) and detached (N-type) cells,[22] the detached cells in the media were transported to a 50-mL tube before detaching the adherent cells by 0.25% trypsin/ethylenediaminetetraacetic acid (Trypsin/EDTA) in the incubator for 1–2 min. The mixture was then neutralised by complete growth media (10% FBS-supplemented media). The detached cells by Trypsin/EDTA were combined with the cells in the 50-mL tube, followed by centrifugation (220 × *g*, 3 min). The resultant cell pellet was resuspended in 1 mL of the FBS-supplemented media. The cell counting was then performed for cell seeding. A cell density of 10,000/cm^2 was seeded in each well of a collagen-I-coated 6-well plate (Gibco A1142801, Thermo Fisher Scientific) for metabolic-based cell viability and proliferation assays or on laminin-coated coverslips (72298-08, Electron Microscopy Sciences, CN Tech Lab Supplies) for immunostaining assays for cell counting and Ki67-cell proliferation indicator. In addition, the cells (10,000/cm^2) were seeded in T25 flasks (25 cm^2) for ELISA quantification of ERK 1/2 (phospho-p44/42 MAPK) proteins in which the culture surfaces were un-coated to ensure the purity of the quantified proteins. Subsequently, the cells were incubated overnight. The cells were then cell-cycle synchronised using the well-documented neurogenic protocol described by Encinas et al.[38] for 12 days (see the flow chart of the neurogenic protocol and LIPUS treatment in Figure 1A). Briefly, the cells

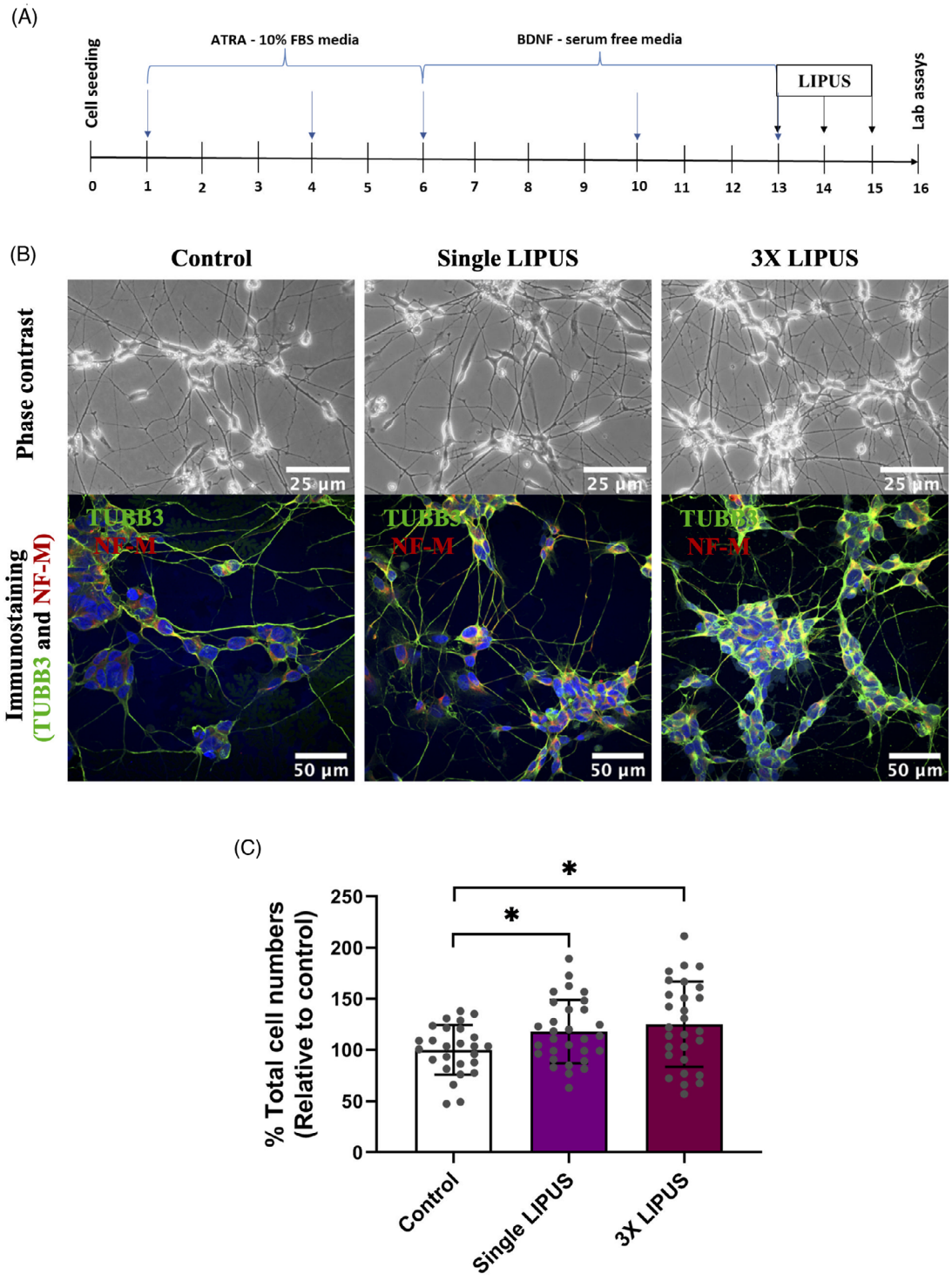

FIGURE 1 Low-intensity pulsed ultrasound (LIPUS) study flow chart and total cell counts of the experimental groups as determined by cell counter image analysis: (A) the schematic diagram illustrating the preparation of the cell culture (blue arrows) and the regimen of the LIPUS exposure (black arrows) throughout the time (days); (B) the experimental groups in phase contrast and immunostaining images: cells were stained with β-tubulin (TUBB3) and neurofilament medium (NF-M) neural markers; (C) the % of total cell numbers – the counting was performed on the immunostaining images in which total number of cells labelled with neural marker (s) per image was counted using cell counter, Fiji ImageJ analysis software. Subsequently, the relative percentage to control was calculated to reveal the difference percentage. All images were captured at a 40× magnification either using phase contrast microscope and/or Zeiss LSM 700 confocal microscopy (multi-track laser scanning mode); scale bars are shown. The data are mean ± standard deviation (SD). Statistical comparisons were performed using one-way ANOVA and then the Games–Howell post hoc test for pairwise comparison (control: $n = 26$, single low-intensity pulsed ultrasound [LIPUS]: $n = 30$; 3× LIPUS: $n = 28$; $^*p \leq .05$).

were treated with ATRA (R 2625, Sigma-Aldrich) in the presence of 10% FBS for 5 days and then treated with BDNF (SRP3014, Sigma-Aldrich; 78005, STEMCELL Technologies) in serum-free media for 7 days. After that, the cells were replenished with fresh BDNF-supplemented serum-free media before starting the LIPUS experiments. All plasticware were purchased from Thermo Scientific, and all materials from Sigma-Aldrich, unless otherwise stated.

2.2 | LIPUS set-up

The LIPUS device (Osteotron IV) was used to deliver LIPUS (the intensity I_{SATA}: 60 mW/cm^2, frequency: 1.5 MHz, pulse repetition: 100 Hz and duty cycle: 20%) for 20 min as previously described with some modifications.[49] The cell culture wells were placed on the top of the transducers with a thin coat of ultrasound transmission gel (Aquasonic 100, Parker Laboratories). To avoid LIPUS wave interference between the LIPUS groups, the only corner wells on each side of 6-well plate were used, whereas the middle wells were untreated and filled with phosphate-buffered saline (PBS). Control groups were cultured in a separate 6-well plate and treated the same way as the LIPUS plates but without actual LIPUS exposure. Thus, the cell cultures were treated with LIPUS stimulation, and the control cell cultures were treated with sham stimulation (LIPUS machine was turned off). The LIPUS treatment was either single or triple exposures (once per day for 3 successive days), in which the treatment was completely conducted in the incubator (37°C, 5% CO_2). After the 3-day LIPUS exposure, the analyses were conducted (Figure 1A). All described steps were gently performed because the SH-SY5Y-derived neural stem cells are small in size and easily disturbed.

2.3 | Immunocytochemistry

The cell cultures were fixed with 4% paraformaldehydefor 10 min. The cells are then only permeabilised for anti-Ki67 intracellular antibody with Triton X-100 (0.5% prepared in PBS) for 10 min. After that, the cell cultures were blocked with blocking solution (10% goat serum, 3% bovine serum albumin [BSA] and 0.1% Triton X-100 prepared in PBS) for 1 h. The cell cultures were then incubated with the diluted primary antibody overnight at 4°C (diluent solution: 3% BSA prepared in PBS with the addition of 0.05% tween-20; see the dilutions and antibodies in Table 1). Negative controls were incubated with blank diluent solution (no antibody addition). Subsequently, all cell cultures were incubated for 1 h with the diluted secondary antibody in a light-protective container (the dilutions and antibodies are presented in Table 1). Finally, the cell cultures were mounted on microscopic slides by a mounting agent with DAPI (Abcam) for nuclear staining. These slides were kept in the light-protective container at 4°C until microscopic scanning using a confocal microscope (Zeiss LSM 700). There was washing step with PBS (3 × 10 min) after all previously mentioned steps except between blocking and primary antibody placement.

2.4 | Cell counting using image analysis

The images of the cells immunostained for the neural markers (β3-tubulin alone or β3-tubulin and neurofilament medium) and proliferation marker (Ki67) were used to count total cell number and Ki67-labelling cells per image of each experimental group. The DAPI-stained nuclei of the cells labelled with neural markers were counted per experimental image using a Cell Counter plugin in Fiji-ImageJ software (https://imagej.nih.gov/ij/plugins/cell-counter.html). The relative percentage was then calculated. Similarly, Ki67-labelling cells and total cell number were counted using the Cell Counter plugin. The proliferation ratio of Ki67-immunopositive cells was then calculated among the total number of DAPI-labelled cells per image. The mean of the cell numbers was computed from random images of the experimental groups.

2.5 | Metabolic-based cell viability and proliferation assays

The cell counting kit-8 (CCK-8) and alamarBlue (AB) assays are metabolic-based assays which were used to estimate cell numbers. These assays were validated for cell proliferation using known cell numbers seeded per well of 96-well plate (39,062.5, 78,125, 156,250 and 312,500/cm^2). The cells were then incubated at 37°C with 5% CO_2 for 6 h to allow cell adherence to the culture surfaces. The assays were then performed according to manufacture instructions. Briefly, cell cultures were incubated either with a 10% final concentration of CCK-8 or AB in blank DMEM/F12 media without any supplements at 37°C with 5% CO_2 for 3 or 3.5 h, respectively. The absorbance was then read using a plate reader (BioTek Instruments; Tecan, ELx800; AB: wavelength of 570 and 600 nm; CCK-8: wavelength of 450 and 460 nm as reference filter).

2.6 | ERK1/2 (p44/42MAPK) signalling

The ERK/MAPK signalling pathway has been involved in LIPUS-promoted cell proliferation of some cell types.[5,50–52]

TABLE 1 Immunofluorescence antibodies and dilutions used.

Antibody	Type	Host species	Description	Dilution	Supplier	Product number
Anti-βIII-tubulin (2G10)	Primary	Mouse	Monoclonal	1:400/500	Abcam/Sigma-Aldrich	ab78078/T8578
Anti-160 kD neurofilament medium	Primary	Rabbit	Polyclonal	1:1000	Abcam	ab9034
Anti-Ki67	Primary	Rabbit	Polyclonal	1:200	Abcam	ab66155
Alexa Fluor 555	Secondary	Goat	Polyclonal	1:500	Abcam	ab150078
Alexa Fluor 488	Secondary	Goat	Monoclonal	1:400	Invitrogen, Thermo Fisher Scientific	A20181

It was of interest to study whether the ERK/MAPK pathway was also involved in LIPUS-promoted neural stem cell proliferation. As both LIPUS exposures (single and 3× LIPUS) were effective in inducing cell proliferation, the single 20-min LIPUS exposure was selected for this investigation.

The cell cultures were supplemented with or without 10 μM U0126 (MEK/ERK inhibitor, Cell Signaling Technology) as previously described[51,53] for 1 h before single LIPUS or sham exposure. The cells were then directly lysed for ELISA quantification of ERK 1/2 (phospho-p44/42 MAPK) or further 48-h incubated for the Ki67-immunostaining assay, which is previously described in immunocytochemistry section. The cell lysis and ELISA work were carried out according to the manufacturer's instructions (PathScan Phospho-p44/42 MAPK: Thr202/Tyr204, Sandwich ELISA Kit, Cell Signaling Technology). Briefly, the cell cultures were immediately rinsed twice with PBS and lysed with lysis solution for 5 min incubated on ice. The lysis solution was supplemented with a protease inhibitor (1 mM phenylmethylsulphonyl fluoride, Sigma-Aldrich) to prevent protein degradation. Subsequently, the lysed cell cultures were sonicated (~30 s) and centrifuged at 14,000 rpm using cold centrifuge (4°C) (Centrifuge 5415R, Eppendorf) for 10 min. The cell lysates were then kept at −80°C until ELISA work.

The Phospho-p44/42 MAPK-coated 96-well plate and the lysates were defrosted at room temperature. Lysate of 100 μL was added per well (duplicate wells per experimental group), sealed and kept overnight at 4°C. A volume of 100 μL detection antibody, HRP-linked secondary antibody and TMB solutions were then sequentially added, sealed and incubated for 1 h, 30 min and 10 min at 37°C and 5% CO_2, respectively. The wells were washed with wash buffer (four times) using an automated well-plate washer (BioTek) after each step. The assay reaction was ended by 100 μL stop solution per well. The absorbance was then read at 450 nm using a microplate reader (Spark, Tecan). The data were normalised to total cell numbers and then expressed as relative percentages to controls.

2.7 | Statistical analysis

All experiments were repeated at least twice with two to four technical replicates per experimental group. Data analysis was performed using IBM SPSS Statistics (version 26). The normality of the data was assessed by Kolmogorov–Smirnov tests. The statistical comparative test was then decided either one-way ANOVA followed by an appropriate post hoc test based on the findings of the homogeneity test of variances for parametric 'normal distributed' data or the Kruskal–Wallis test followed by the Bonferroni post hoc test for nonparametric 'non-normal distributed' data. These were the main statistical tests to compare between the experimental groups unless otherwise stated. The statistical significance level was set at $p \leq .05$. The data were shown as mean ± standard deviation unless otherwise stated. The bar graphs were created using GraphPad Prism 9.

3 | RESULTS

3.1 | LIPUS increased cell numbers

Phase contrast and immunostaining images of the experimental groups clearly demonstrated that the LIPUS-induced groups exhibited a higher neural stem cell population compared with control group (Figure 1B). The immunostained images (β-tubulin [TUBB3] and neurofilament medium [NF-M] immunopositive) were chosen for cell counting using the cell counter, Fiji-ImageJ analysis software. The percentage mean average for the control group was 100 ± 24.27, whereas the single LIPUS and 3× LIPUS groups demonstrated a mean average of 117.81 ± 30.96 and 125.08 ± 41.65, respectively. Statistically, the data revealed that a significant difference was evident in cell numbers between the groups (Figure 1C; one-way ANOVA test, *F*-statistics (df): F (2.81) = 4.046, $p = .021$). LIPUS-induced groups demonstrated higher statistically significant cell numbers than the control group

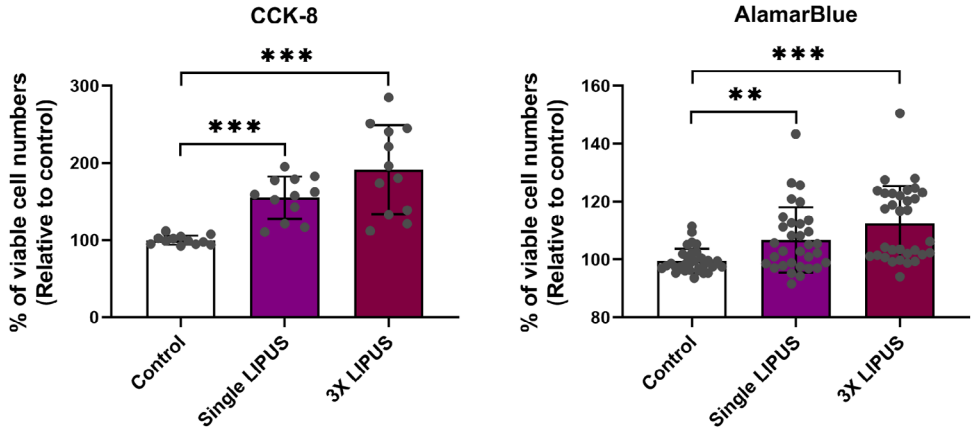

FIGURE 2 Assessment of cell numbers as determined by cell counting kit-8 (CCK-8) and alamarBlue (AB) assays: (A) CCK-8 assay – the relative percentage of CCK-8 absorbance levels (% viable cell numbers); (B) AB assay – the relative percentage of AB reduction levels (% viable cell numbers). The data are presented as mean ± standard deviation (SD). The statistical comparison was performed using the Kruskal–Wallis test with pairwise comparison; the significance values were adjusted by the Bonferroni correction for multiple tests (AB: $n = 32$, CCK-8 assay: $n = 12$; *$p \leq .05$, **$p \leq .01$ and ***$p \leq .001$).

(Figure 1C; $p = .050$ for control vs. single LIPUS and $p = .024$ for control vs. 3× LIPUS). The 3× LIPUS group demonstrated relatively higher cell numbers compared with single LIPUS group; however, this difference was not significant (Figure 1C: $p = .734$). These findings suggest that LIPUS promoted cell proliferation. Next, we explored whether the LIPUS-induced increase in cell numbers was reflected by overall increase in viable cell numbers of the cell population.

3.2 | LIPUS increased viable cell numbers

Two 'metabolic' viability assays (CCK-8 and AB) were validated, and data showed a linear relationship (R^2 coefficient >.9) between the cell seeding numbers and absorbance levels of both metabolic-based assays. This means the increase in absorbance values reflected the increase in viable cell numbers per experimental group (Supporting information file). Consequently, both metabolic assays demonstrated that LIPUS significantly increased the viable cell numbers (CCK-8 assay: one-way ANOVA F ratio (df) = 18.607 (2,33), $p < .001$; AB assay: Kruskal-Wallis test - test statistics (df) = 24.801 (2), $p < .001$). The single LIPUS group (20-min exposure) demonstrated significantly greater levels of cell-count absorbance than control group (Figure 2; CCK-8 assay: $p < .001$and AB assay: $p = .009$). The 3X LIPUS group (once per day for 3 successive days) resulted in a further significant difference in levels of the cell-count absorbance compared with the control/sham group (CCK-8 and AB assays: $p < .001$). The 3× LIPUS group was also higher than single LIPUS group assessed by both assays, but there was no statistically significant difference (Figure 2; CCK-8 assay: $p = .147$ and AB assay: $p = .138$) underscoring the image analysis data of the immunostained cells. Next, we examined whether the increase in cell numbers was in fact caused by increase in cell proliferation.

3.3 | LIPUS-increased neural stem cell numbers were due to increased cell proliferation as evidenced by Ki67-cell proliferation indicator

The immunocytochemical data demonstrated that both LIPUS groups exhibited a greater number of Ki67-positive nuclei cells than control group indicating that the increase in neural stem cells is due to an increase in cell proliferation. However, the 3× LIPUS group exhibited the greatest Ki67-positive cells (Figure 3A). The statistical analysis demonstrated that there is a statistical difference in the number of Ki67-positive nuclei cells (Kruskal–Wallis test – test statistics (df) = 46.509 (2), $p < .001$). In line with the previous data, the numbers of Ki67-positive nuclei cells in the LIPUS groups were statistically higher than control group (Figure 3B: adjusted p value <.001). The 3× LIPUS group had the greatest numbers of Ki67-positive cells, albeit not statistically different compared with the single LIPUS group (adjusted $p = .588$). The proliferation ratio (Ki67-staining index) also revealed a statistically significant difference between the groups (Kruskal–Wallis test – test statistics (df) = 44.842 (2), $p < .001$). Both single and 3× LIPUS groups demonstrated significantly greater percentage of Ki67-positive cells than control group (Figure 3B: adjusted $p < .001$). No significant difference was detected between the single and 3× LIPUS groups (adjusted $p = 1$).

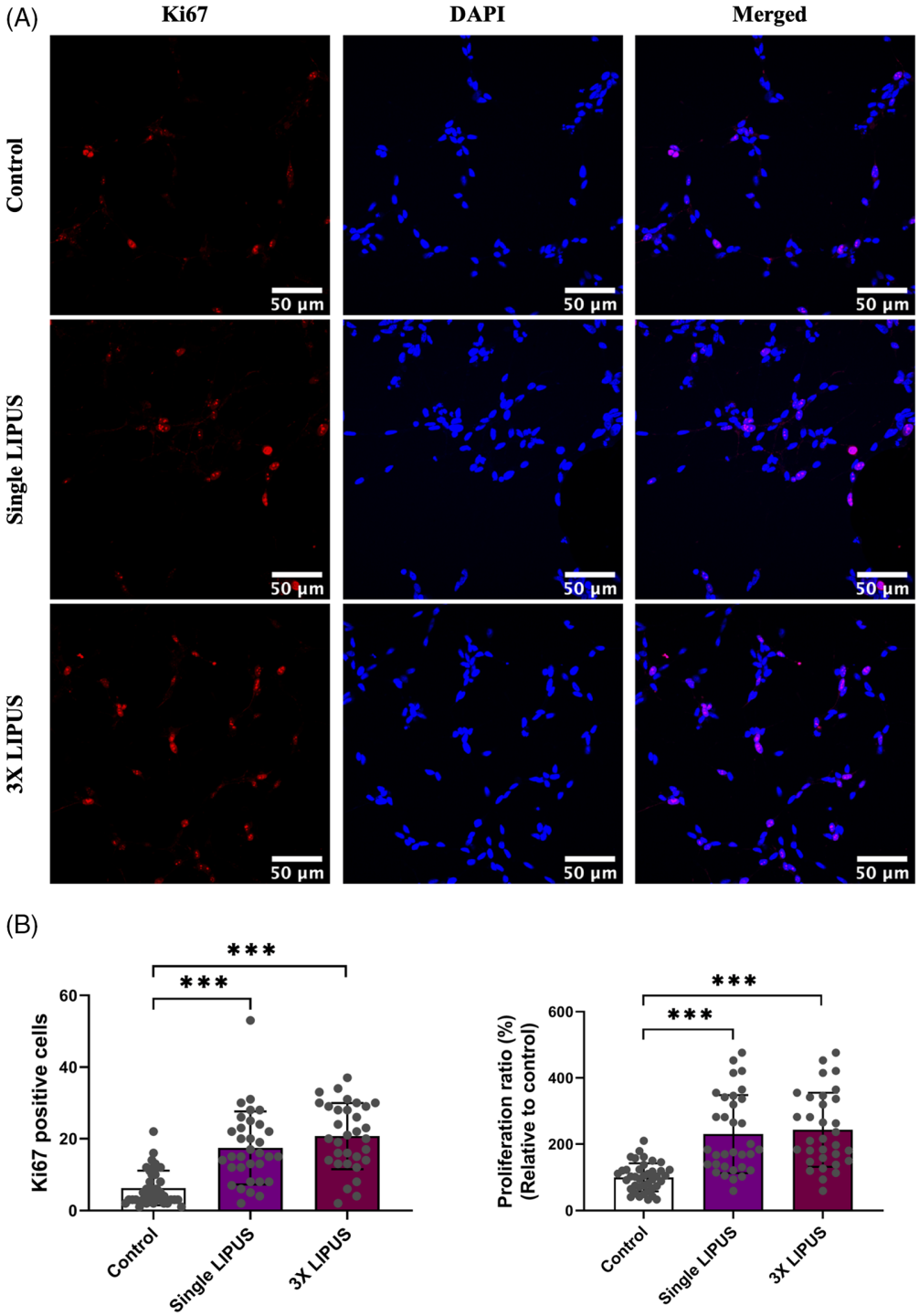

FIGURE 3 Immunocytochemical analysis of the Ki67-proliferative nuclear protein marker in the SH-SY5Y-neural stem cells: (A) representative immunocytochemical images – the Ki67 marker stains the nuclei of newly formed cells (red) and DAPI dye stains all nuclei (blue). Images were captured with oil lens at a 40× magnification using multi-track laser scanning of the Zeiss LSM 700 confocal microscopy; scale bars are shown. The images were adjusted to increase colour contrast for visibility using the brightness/contrast tool in Fiji ImageJ software; (B) Ki67-immunopositive cells and their proliferation ratio – the Ki67-stained cells were counted, and their percentage in the whole cell population (stained by DAPI) per image was calculated. The plotted data are mean ± standard deviation (SD). The statistical comparison was performed using the Kruskal–Wallis test with pairwise comparison; the significance values were adjusted by the Bonferroni correction for multiple tests (control: $n = 40$, single low-intensity pulsed ultrasound [LIPUS]: $n = 33$; 3× LIPUS: $n = 32$, ***$p \leq .001$).

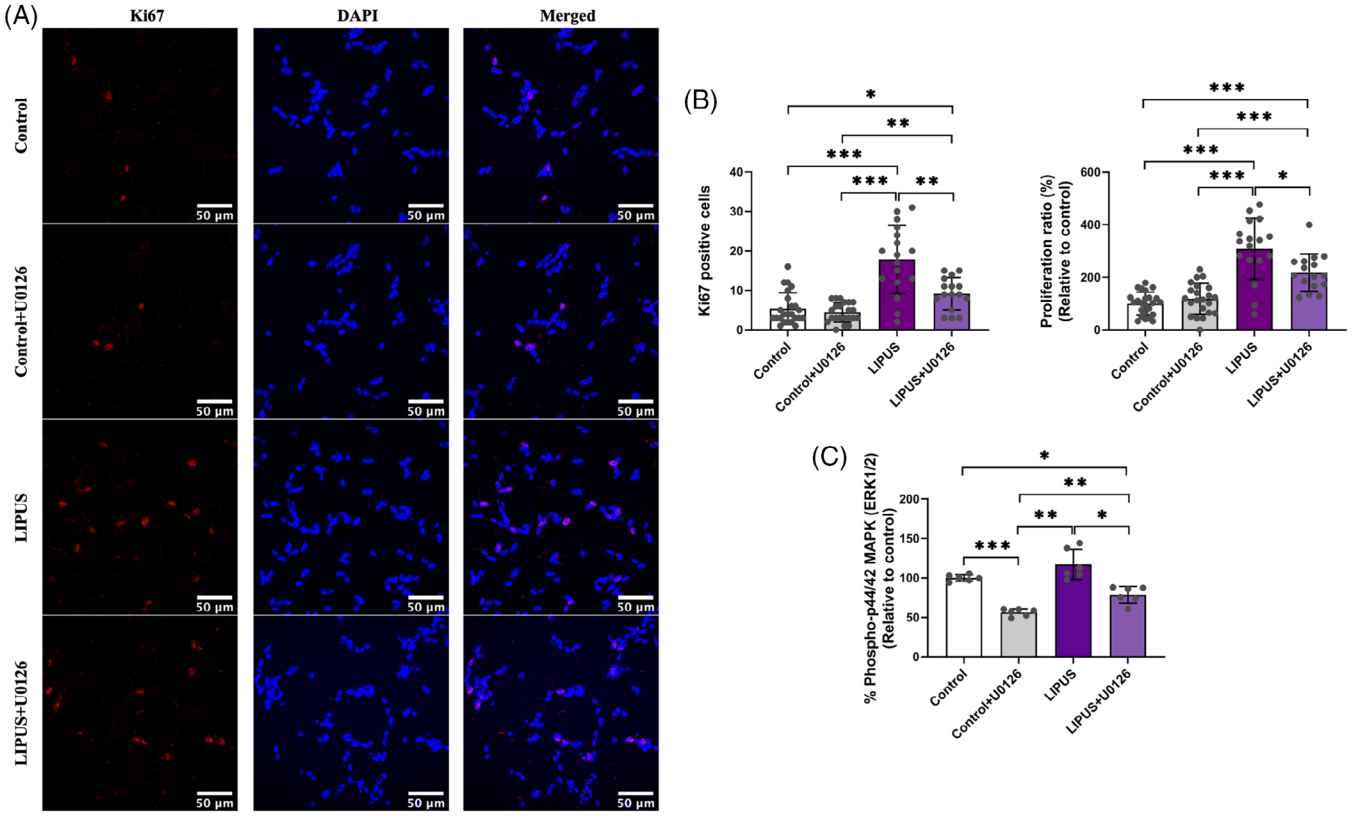

FIGURE 4 The Ki67-labelled proliferation and phospho-ERK1/2 protein levels with and without the MEK/ERK inhibitor (U0126): (A) representative Ki67-immunostained images of the experimental groups – the nuclei of the newly formed cells were stained with the Ki67 marker (red stain), whereas the nuclei of whole cell population were stained with the DAPI (blue stain). Images were captured at a 40× magnification using Zeiss LSM 700 confocal microscopy (multi-track laser scanning mode). The images were adjusted to increase colour contrast for visibility using brightness/contrast tool in Fiji ImageJ software; (B) the absolute Ki67-cell counts and their proliferation ratio – the Ki67-immunopositive cells were counted, and then the relative percentage of the Ki67-immunopositive stained cells to the whole cell population per captured image was calculated; (C) the quantification of phosho-ERK1/2 protein levels – these data were quantified by quantitative sandwich ELISA. The plotted data are mean ± standard deviation (SD). The statistical comparison was performed using one-way ANOVA, and then the Gabriel post hoc test was used to compare between the experimental groups of the Ki67-positive cells (data were transformed into normally distributed data using the square root method), whereas the Games–Howell post hoc test was used to compare between the experimental groups of the proliferation ratio and phospho-ERK1/2 data (Ki67-positive cells and proliferation ratio: control, $n = 24$; control + U0126, $n = 22$; low-intensity pulsed ultrasound [LIPUS], $n = 17$, LIPUS + U0126, $n = 16$; phospho-ERK1/2: $n = 6$; *$p \leq .05$, **$p \leq .01$ and ***$p \leq .001$).

Next, it was of interest to examine if ERK/MAPK signalling was involved in the LIPUS-promoted neural stem cell proliferation.

3.4 | ERK/MAPK signalling was involved in LIPUS-induced neural stem cell proliferation

The immunostaining demonstrated that the increase of Ki67-lablelled cells in the LIPUS-induced groups was noticeably reduced after U0126 pre-treatment (MEK/ERK inhibitor). However, the LIPUS with U0126 group still displayed greater Ki67 levels than control groups with and without U0126 (Figure 4A). Statistically, the data confirmed that there is a highly significant difference in Ki67-stained cell numbers (one-way ANOVA: F ratio (df) = 22.697 (3,75), $p < .001$) and in proliferation ratio (one-way ANOVA: F ratio (df) = 33.185 (3,75), $p < .001$). In this context, the LIPUS-induced group exhibited statistically greater Ki67-positive nuclei and proliferation ratio than LIPUS with U0126 group (Figure 4B, Ki67 numbers: $p = .002$; proliferation ratio: $p = .050$) and control groups ($p < .001$). In contrast, no statistical difference in the Ki67-cell numbers or proliferation ratio was detected between the control groups with and without U0126 (Figure 4B, Ki67 numbers: $p = .969$; proliferation ratio: $p = .658$). Surprisingly, the LIPUS with U0126 group demonstrated significant greater Ki67-cell numbers and proliferation ratio than the control group (Figure 4B, Ki67 numbers:

$p = .041$; proliferation ratio: $p < .001$), and control with U0126 group (Ki67 numbers: $p = .006$; proliferation ratio: $p < .001$).

The ERK/MAPK ELISA revealed similar results to the Ki67 staining, demonstrating that the LIPUS-induced groups exhibited the highest phospho-ERK1/2 levels among the tested groups, and the U0126 pre-treatment lowered the levels of the phospho-ERK1/2 proteins (Figure 4C). Statistically, a high significant difference between the tested groups was detected (one-way ANOVA test, F-statistics (df) = 32.079 (3,20), $p < .001$). Although LIPUS-induced group showed a noticeable increase in phospho-ERK1/2 proteins compared to the control group, this increase was not statistically different (Figure 4C, $p = .247$). However, the significant upregulated levels of phospho-ERK1/2 proteins were detected in the LIPUS-promoted group compared with the control with U0126 ($p = .002$), and LIPUS with U0126 ($p = .012$) groups (Figure 4C). Likewise, the U0126-treated groups (control with U0126 and LIPUS with U0126) showed a significant reduction in levels of phospho-ERK1/2 proteins compared to the control group (control with U0126 vs. control: $p < .001$; LIPUS with U0126 vs. control: $p = .013$). Notably, the LIPUS with U0126 group resulted in significantly greater phospho-ERK1/2 levels than control with U0126 group (Figure 4C, $p = .010$). Taken together, these data indicate the involvement of the ERK/MAPK signalling and possibility of involvement of other upstream regulator(s) 'beside to MEK1/2 regulator' for ERK phosphorylation in the LIPUS-induced neural stem cell proliferation.

4 | DISCUSSION

The present study demonstrated that LIPUS exposure induces cell proliferation of neural stem cells established from human-derived SH-SY5Y cells. This study also shows that the ERK1/2 signalling may play a significant role in the proliferative process of LIPUS on the neural stem cells. These novel findings imply that therapeutic LIPUS can trigger the cell proliferation of human neural stem cells.

The data of the cell counting and viable cell number assays corresponded with the Ki67-cell proliferation marker[54] underscoring the cell proliferative effect of LIPUS on the neural stem cell cultures. The findings are consistent with other LIPUS studies on various cell types as assessed by cell viability assays[13,20,51,55–58] and proliferation indicators,[20,51,52,55,59] which reported a significant increase in cell numbers and/or higher cell viability after LIPUS treatment. Similarly, the present study agrees with results of previous studies using various neural stem cell types such as the cell viability of SH-SY5Y cells[60] and the cell proliferation of iPSC-derived and rat neural stem cells.[15,20] However, there are differences in LIPUS settings, in particular, the effective LIPUS intensity dose to increase cell viability and/or proliferation of neural stem cells. For example, Guo et al.[60] reported that LIPUS induces a significant increase in the cell viability of SH-SY5Y cells at lower intensity dose (15 mW/cm^2) compared with the present study (60 mW/cm^2). In contrast, Lv et al.[20] and Wu et al.[15] reported that higher intensities of LIPUS (500 and 69.3 mW/cm^2) compared with the present study (60 mW/cm^2) produce a significant increase in cell proliferation of iPSC-derived and rat neural stem cells. There are also differences in the other LIPUS parameters such as much higher pulse repetition rate (1 KHz) in the study of Guo et al.[60] and lower frequencies (1 MHz) in the study of Lv et al.[20] and Wu et al.[15] compared with the present study (pulse repetition rate: 100 Hz; frequency: 1.5 MHz). Hence, the effective LIPUS intensity dose may vary according to other LIPUS parameters used. In other words, when high pulse repetition or frequency is used, lower intensity is selected and vice versa. Regarding the intensity dose (60 mW/cm^2) used in the present study, it has also been reported as an effective dose that induces cell proliferation and/or regeneration of cartilage[49,61] and muscle cells.[62] Overall, regardless of the differences in cell types and LIPUS settings, the consistency in the results of the studies suggests that the LIPUS can promote neural stem cell proliferation.

Considering the agreement in the increase of the viable cells assessed by metabolic assays, it indicates that LIPUS might stimulate metabolic activities which subsequently result in cell proliferation. This interpretation agrees with Huang et al.[63] who reported that the metabolite compositions and genes have a significant role in regulating cell proliferation induced by LIPUS. Another interpretation of the LIPUS-induced cell proliferation was highlighted by He et al.,[64] Xie et al.[57] and Ling et al.[51] who reported that LIPUS drives the stem cells from the 'stationary phase' into the 'proliferative phase' of the cell cycle, resulting in cell proliferation. Similarly, Hu et al.[58] showed that LIPUS produced greater cell viability of cardiomyocytes through entering the active cell cycles 'S and G2/M phases' from the stationary phase 'G0/G1 phase'. In this context, the SH-SY5Y-derived neural stem cells used in this study have been reported to be arrested in the 'stationary G1 phase' of the cell cycle after neurogenic induction.[38] Interestingly, the G1 phase can be stimulated(s) to re-enter the active cell cycle and proliferate or lengthen the phase for neurogenesis, as reported in some studies.[65–67] In addition, the SH-SY5Y-derived neural stem cells can still proliferate after neurogenic induction, but in much lower rate compared with un-induced cells.[38,44,45] Hence, the proliferated cells in this study might be either pre-existing neural stem cells or activated neurogenic-induced neural stem cells.

The results demonstrated that the MEK/ERK inhibitor (U0126) significantly reduced the neural stem cell proliferation (Ki67-labelled cells) and ERK phosphorylation induced by LIPUS, which indicates involvement of ERK/MAPK signalling. These results agree with some studies that highlighted the role of ERK signalling in LIPUS-promoted cell proliferation.[5,50–52] In this context, it would be interesting to investigate the dose-dependent effect of the MEK/ERK inhibitor (U0126) to elucidate whether certain inhibitor concentration(s) can fully block LIPUS-induced ERK phosphorylation and cell proliferation (Ki67-labelled cells) without affecting the cell proliferation of LIPUS-untreated cells. Unexpectedly, the control group with MEK/ERK inhibitor demonstrated a decrease in phospho-ERK levels, but this decrease was not associated with any significant change in Ki67-cell proliferation. These results indicate the phospho-ERK decrease of the controls is not related to the cell proliferation. As the ERK signalling pathway is central for multiple biological processes,[68] it justifies the decrease in phospho-ERK levels of the controls with MEK/ERK inhibitor. Furthermore, the LIPUS with the MEK/ERK inhibitor group showed significantly higher cell proliferation and ERK phosphorylation than the control with MEK/ERK inhibitor group. This suggests that the LIPUS-promoted cell proliferation and ERK phosphorylation are partially inhibited by MEK/ERK inhibitor, and other upstream signalling inducer(s) may be involved in this process. This interpretation is consistent with Zhou et al.[50] who reported that there is another upstream regulator (ROCK/Rho) besides the MEK regulator triggering ERK phosphorylation and cell proliferation activated by LIPUS. In addition, it has been highlighted that other regulators rather than the classical 'MEK–ERK cascade' can trigger ERK/MAPK signalling.[68,69] Taken together, LIPUS may stimulate more than one upstream regulator inducing ERK signalling in SH-SY5Y cells. Moreover, as multiple signalling pathways are elicited by LIPUS such as PI3K-Akt and ERK/MAPK,[51] ERK, JNK or JNK and p38,[52] ERK, JNK and p38 MAPK,[70] PI3K-Akt,[59] notch,[15] GSK-3β/β-catenin,[13] and PI3K-Akt and JNK MAPK,[55] Ca 2^+ signalling,[11] further investigations are required to reveal all involved signalling pathways induced by LIPUS and their interplays in the neural stem cells. In this context, advanced techniques such as proteomic quantification[71,72] or genomic techniques[73,74] can be used to reveal all involved pathways, their regulators and their interplays.

Regarding possible clinical translation of the present research, LIPUS may be effective as a sole therapeutic tool or combined with another therapeutic approach such as microbubbles, which has been reported to enhance the LIPUS effects on cell proliferation and differentiation[75–77] and neovascularisation,[78] for stem cell therapy and tissue engineering approaches in the regenerative medicine. More specifically related to the present study, the LIPUS-induced cell proliferation of neural stem cells would benefit nerve repair and regeneration approaches like induction of nerve supply for regenerative endodontic treatment and management of traumatic nerve injuries.

Despite the best efforts, this study has a potential limitation. Although the SH-SY5Y-derived neural model showed neural features and simulated neural stem cells, it may not accurately represent the primary human neural stem cells and their physiological conditions. Thus, further in vivo studies are required to evaluate LIPUS effects on human neuromodulation.

The present study demonstrates that LIPUS exposure is able to stimulate cell proliferation of the human neural stem cells, which seems to be in part mediated by the ERK/MAPK signalling pathway. LIPUS may be a suitable non-invasive therapeutic tool to stimulate neural stem cell expansion in nerve repair and regeneration. Further studies are required to reinforce the clinical translation of the application(s) of LIPUS.

AUTHOR CONTRIBUTIONS

Conception; methodology; data interpretation; Final approval of the version: Arwa A. Al-Maswary, A. Damien Walmsley, Paul R. Cooper and Ben A. Scheven. *Investigation and data collection; data analysis; visualisation (images and graphs); writing – drafting*: Arwa A. Al-Maswary. *Supervision; writing—revision and editing*: A. Damien Walmsley, Paul R. Cooper and Ben A. Scheven.

ACKNOWLEDGEMENTS

Special thanks to Gay Smith, Michelle Holder and Helen Wright for their technical assistance and advice during the laboratory work of this study at School of Dentistry, University of Birmingham. Authors wish to thank Dr Huzaimi Haron, PhD student from School of Pharmacy, University of Birmingham for donating SH-SY5Y neuroblastoma cell line.

CONFLICT OF INTEREST STATEMENT

The authors declare that no conflicts of interest exist.

FUNDING INFORMATION

IsDB Merit Scholarship, IDB/Grant No. 600031755; School of Dentistry—University of Birmingham, Grant No. GAM2271

DATA AVAILABILITY STATEMENT

Data are available upon reasonable request.

ETHICS STATEMENT

Not applicable

ORCID

Arwa A. Al-Maswary https://orcid.org/0000-0003-4310-4742

REFERENCES

1. de Lucas B, Pérez LM, Bernal A, Gálvez BG. Ultrasound therapy: experiences and perspectives for regenerative medicine. *Genes (Basel)*. 2020;11(9):1086.
2. Tanaka E, Kuroda S, Horiuchi S, Tabata A, El-Bialy T. Low-intensity pulsed ultrasound in dentofacial tissue engineering. *Ann Biomed Eng*. 2015;43(4):871-886.
3. Rubin C, Bolander M, Ryaby JP, Hadjiargyrou M. The use of low-intensity ultrasound to accelerate the healing of fractures. *J Bone Joint Surg Am*. 2001;83(2):259-270.
4. Ning GZ, Song WY, Xu H, et al. Bone marrow mesenchymal stem cells stimulated with low-intensity pulsed ultrasound: better choice of transplantation treatment for spinal cord injury: treatment for SCI by LIPUS-BMSCs transplantation. *CNS Neurosci Ther*. 2019;25(4):496-508.
5. Xia B, Chen G, Zou Y, Yang L, Pan J, Lv Y. Low-intensity pulsed ultrasound combination with induced pluripotent stem cells-derived neural crest stem cells and growth differentiation factor 5 promotes sciatic nerve regeneration and functional recovery. *J Tissue Eng Regen Med*. 2019;13(4):625-636.
6. Jiang W, Wang Y, Tang J, et al. Low-intensity pulsed ultrasound treatment improved the rate of autograft peripheral nerve regeneration in rat. *Sci Rep*. 2016;6:22773.
7. Sato M, Motoyoshi M, Shinoda M, Iwata K, Shimizu N. Low-intensity pulsed ultrasound accelerates nerve regeneration following inferior alveolar nerve transection in rats. *Eur J Oral Sci*. 2016;124(3):246-250.
8. Yang B, Wu Q, Zhang L, Guo Y, Gong P. Effect of low-intensity pulsed ultrasound on the mandibular remodeling following inferior alveolar nerve transection. *Zhongguo Yi Xue Ke Xue Yuan Xue Bao*. 2017;39(2):215-224.
9. Tsuchimochi A, Endo C, Motoyoshi M, et al. Effect of low-intensity pulsed ultrasound on orofacial sensory disturbance following inferior alveolar nerve injury: role of neurotrophin-3 signaling. *Eur J Oral Sci*. 2021;129(5):e12810.
10. Wang T, Ito A, Xu S, Kawai H, Kuroki H, Aoyama T. Low-intensity pulsed ultrasound prompts both functional and histologic improvements while upregulating the brain-derived neurotrophic factor expression after sciatic crush injury in rats. *Ultrasound Med Biol*. 2021;47(6):1586-1595.
11. Truong TT, Chiu WT, Lai YS, Huang H, Jiang X, Huang CC. Ca(2+) signaling-mediated low-intensity pulsed ultrasound-induced proliferation and activation of motor neuron cells. *Ultrasonics*. 2022;124:106739.
12. Zhao L, Feng Y, Hu H, Shi A, Zhang L, Wan M. Low-intensity pulsed ultrasound enhances nerve growth factor-induced neurite outgrowth through mechanotransduction-mediated ERK1/2-CREB-Trx-1 signaling. *Ultrasound Med Biol*. 2016;42(12):2914-2925.
13. Ren C, Chen X, Du N, et al. Low-intensity pulsed ultrasound promotes Schwann cell viability and proliferation via the GSK-3β/β-catenin signaling pathway. *Int J Biol Sci*. 2018;14(5):497-507.
14. Yue Y, Yang X, Zhang L, et al. Low-intensity pulsed ultrasound upregulates pro-myelination indicators of Schwann cells enhanced by co-culture with adipose-derived stem cells. *Cell Prolif*. 2016;49(6):720-728.
15. Wu Y, Gao Q, Zhu S, et al. Low-intensity pulsed ultrasound regulates proliferation and differentiation of neural stem cells through notch signaling pathway. *Biochem Biophys Res Commun*. 2020;526(3):793-798.
16. Monteggia LM, Heimer H, Nestler EJ. Meeting report: can we make animal models of human mental illness? *Biol Psychiatry*. 2018;84(7):542-545.
17. Zhao X, Bhattacharyya A. Human models are needed for studying human neurodevelopmental disorders. *Am J Hum Genet*. 2018;103(6):829-857.
18. Ransohoff RM. All (animal) models (of neurodegeneration) are wrong. Are they also useful? *J Exp Med*. 2018;215(12):2955-2958.
19. Jansen K, Pou Casellas C, Groenink L, Wever KE, Masereeuw R. Humans are animals, but are animals human enough? A systematic review and meta-analysis on interspecies differences in renal drug clearance. *Drug Discovery Today*. 2020;25(4):706-717.
20. Lv Y, Zhao P, Chen G, Sha Y, Yang L. Effects of low-intensity pulsed ultrasound on cell viability, proliferation and neural differentiation of induced pluripotent stem cells-derived neural crest stem cells. *Biotechnol Lett*. 2013;35(12):2201-2212.
21. Lv Y, Nan P, Chen G, Sha Y, Xia B, Yang L. In vivo repair of rat transected sciatic nerve by low-intensity pulsed ultrasound and induced pluripotent stem cells-derived neural crest stem cells. *Biotechnol Lett*. 2015;37(12):2497-2506.
22. Kovalevich J, Langford D. Considerations for the use of SH-SY5Y neuroblastoma cells in neurobiology. *Methods Mol Biol*. 2013;1078:9-21.
23. Gordon J, Amini S, White MK. General overview of neuronal cell culture. *Methods Mol Biol*. 2013;1078:1-8.
24. Biedler JL, Helson L, Spengler BA. Morphology and growth, tumorigenicity, and cytogenetics of human neuroblastoma cells in continuous culture. *Cancer Res*. 1973;33(11):2643-2652.
25. Ioghen OC, Ceafalan LC, Popescu BO. SH-SY5Y cell line in vitro models for Parkinson disease research-old practice for new trends. *J Integr Neurosci*. 2023;22(1):20.
26. Lopez-Suarez L, Awabdh SA, Coumoul X, Chauvet C. The SH-SY5Y human neuroblastoma cell line, a relevant in vitro cell model for investigating neurotoxicology in human: focus on organic pollutants. *Neurotoxicology*. 2022;92:131-155.
27. Loser D, Hinojosa MG, Blum J, et al. Functional alterations by a subgroup of neonicotinoid pesticides in human dopaminergic neurons. *Arch Toxicol*. 2021;95(6):2081-2107.
28. Biedler JL, Roffler-Tarlov S, Schachner M, Freedman LS. Multiple neurotransmitter synthesis by human neuroblastoma cell lines and clones. *Cancer Res*. 1978;38(11 Part 1):3751-3757.
29. Gatta V, Drago D, Fincati K, et al. Microarray analysis on human neuroblastoma cells exposed to aluminum, β(1-42)-amyloid or the β(1-42)-amyloid aluminum complex. *PLoS One*. 2011;6(1):e15965.
30. Zhang Z, Hou L, Li X, et al. Neuroprotection of inositol hexaphosphate and changes of mitochondrion mediated apoptotic pathway and α-synuclein aggregation in 6-OHDA induced Parkinson's disease cell model. *Brain Res*. 2016;1633:87-95.
31. Wang S, Xia B, Qiao Z, et al. Tetramethylpyrazine attenuated bupivacaine-induced neurotoxicity in SH-SY5Y cells through regulating apoptosis, autophagy and oxidative damage. *Drug Des Devel Ther*. 2019;13:1187-1196.

32. Ng YW, Say YH. Palmitic acid induces neurotoxicity and glia-toxicity in SH-SY5Y human neuroblastoma and T98G human glioblastoma cells. *PeerJ*. 2018;6:e4696.
33. Forster JI, Köglsberger S, Trefois C, et al. Characterization of differentiated SH-SY5Y as neuronal screening model reveals increased oxidative vulnerability. *J Biomol Screen*. 2016;21(5):496-509.
34. Orqueda AJ, Gatti CR, Ogara MF, Falzone TL. SOX-11 regulates LINE-1 retrotransposon activity during neuronal differentiation. *FEBS Lett*. 2018;592(22):3708-3719.
35. Al-Maswary AA, O'Reilly M, Holmes AP, Walmsley AD, Cooper PR, Scheven BA. Exploring the neurogenic differentiation of human dental pulp stem cells. *PLoS One*. 2022;17(11): e0277134.
36. Pires AO, Neves-Carvalho A, Sousa N, Salgado AJ. The secretome of bone marrow and wharton jelly derived mesenchymal stem cells induces differentiation and neurite outgrowth in SH-SY5Y cells. *Stem Cells Int*. 2014;2014:438352.
37. Gervois P, Wolfs E, Dillen Y, et al. Paracrine maturation and migration of SH-SY5Y cells by dental pulp stem cells. *J Dent Res*. 2017;96(6):654-662.
38. Encinas M, Iglesias M, Liu Y, et al. Sequential treatment of SH-SY5Y cells with retinoic acid and brain-derived neurotrophic factor gives rise to fully differentiated, neurotrophic factor-dependent, human neuron-like cells. *J Neurochem*. 2000;75(3):991-1003.
39. Agholme L, Lindstrom T, Kagedal K, Marcusson J, Hallbeck M. An in vitro model for neuroscience: differentiation of SH-SY5Y cells into cells with morphological and biochemical characteristics of mature neurons. *J Alzheimers Dis*. 2010;20(4):1069-1082.
40. Kovalevich J, Santerre M, Langford D. Considerations for the use of SH-SY5Y neuroblastoma cells in neurobiology. *Methods Mol Biol*. 2021;2311:9-23.
41. Xie HR, Hu LS, Li GY. SH-SY5Y human neuroblastoma cell line: in vitro cell model of dopaminergic neurons in Parkinson's disease. *Chin Med J (Engl)*. 2010;123(8):1086-1092.
42. Hadfield JD, Sokhi S, Chan GK. Cell synchronization techniques for studying mitosis. *Methods Mol Biol*. 2022;2579:73-86.
43. Wee P, Wang RC, Wang Z. Synchronization of HeLa cells to mitotic subphases. *Methods Mol Biol*. 2022;2579:99-110.
44. Martin ER, Gandawijaya J, Oguro-Ando A. A novel method for generating glutamatergic SH-SY5Y neuron-like cells utilizing B-27 supplement. *Front Pharmacol*. 2022;13:943627.
45. Pahlman S, Ruusala AI, Abrahamsson L, Mattsson ME, Esscher T. Retinoic acid-induced differentiation of cultured human neuroblastoma cells: a comparison with phorbolester-induced differentiation. *Cell Differ*. 1984;14(2):135-144.
46. Teppola H, Sarkanen JR, Jalonen TO, Linne ML. Morphological differentiation towards neuronal phenotype of SH-SY5Y neuroblastoma cells by estradiol, retinoic acid and cholesterol. *Neurochem Res*. 2016;41(4):731-747.
47. Goldie BJ, Barnett MM, Cairns MJ. BDNF and the maturation of posttranscriptional regulatory networks in human SH-SY5Y neuroblast differentiation. *Front Cell Neurosci*. 2014;8:325.
48. Sahin M, Oncu G, Yilmaz MA, Ozkan D, Saybasili H. Transformation of SH-SY5Y cell line into neuron-like cells: investigation of electrophysiological and biomechanical changes. *Neurosci Lett*. 2021;745:135628.
49. Nishida T, Kubota S, Aoyama E, Yamanaka N, Lyons KM, Takigawa M. Low-intensity pulsed ultrasound (LIPUS) treatment of cultured chondrocytes stimulates production of CCN family protein 2 (CCN2), a protein involved in the regeneration of articular cartilage: mechanism underlying this stimulation. *Osteoarthritis Cartilage*. 2017;25(5):759-769.
50. Zhou S, Schmelz A, Seufferlein T, Li Y, Zhao J, Bachem MG. Molecular mechanisms of low intensity pulsed ultrasound in human skin fibroblasts. *J Biol Chem*. 2004;279(52):54463-54469.
51. Ling L, Wei T, He L, et al. Low-intensity pulsed ultrasound activates ERK1/2 and PI3K-Akt signalling pathways and promotes the proliferation of human amnion-derived mesenchymal stem cells. *Cell Prolif*. 2017;50(6):e12383. 10.1111/cpr.12383
52. Gao Q, Walmsley AD, Cooper PR, Scheven BA. Ultrasound stimulation of different dental stem cell populations: role of mitogen-activated protein kinase signaling. *J Endod*. 2016;42(3):425-431.
53. Wang JW, Li YJ, Wu HH, et al. The essential role of the ERK activation in large T antigen of BK polyomavirus regulated cell migration. *Virus Res*. 2023;336:199220.
54. Miller I, Min M, Yang C, et al. Ki67 is a graded rather than a binary marker of proliferation versus quiescence. *Cell Rep*. 1105;24(5):1105-1112.
55. Leng X, Shang J, Gao D, Wu J. Low-intensity pulsed ultrasound promotes proliferation and migration of HaCaT keratinocytes through the PI3K/AKT and JNK pathways. *Braz J Med Biol Res*. 2018;51(12):e7862.
56. Alvarenga EC, Rodrigues R, Caricati-Neto A, Silva-Filho FC, Paredes-Gamero EJ, Ferreira AT. Low-intensity pulsed ultrasound-dependent osteoblast proliferation occurs by via activation of the P2Y receptor: role of the P2Y1 receptor. *Bone*. 2010;46(2):355-362.
57. Xie S, Jiang X, Wang R, et al. Low-intensity pulsed ultrasound promotes the proliferation of human bone mesenchymal stem cells by activating PI3K/AKt signaling pathways. *J Cell Biochem*. 2019;120(9):15823-15833.
58. Hu Y, Jia Y, Wang H, et al. Low-intensity pulsed ultrasound promotes cell viability and inhibits apoptosis of H9C2 cardiomyocytes in 3D bioprinting scaffolds via PI3K-Akt and ERK1/2 pathways. *J Biomater Appl*. 2022;37(3):402-414.
59. Takeuchi R, Ryo A, Komitsu N, et al. Low-intensity pulsed ultrasound activates the phosphatidylinositol 3 kinase/Akt pathway and stimulates the growth of chondrocytes in three-dimensional cultures: a basic science study. *Arthritis Res Ther*. 2008;10(4):R77.
60. Guo H, Baker G, Hartle K, et al. Exploratory study on neurochemical effects of low-intensity pulsed ultrasound in brains of mice. *Med Biol Eng Comput*. 2021;59(5):1099-1110.
61. Kobayashi Y, Sakai D, Iwashina T, Iwabuchi S, Mochida J. Low-intensity pulsed ultrasound stimulates cell proliferation, proteoglycan synthesis and expression of growth factor-related genes in human nucleus pulposus cell line. *Eur Cell Mater*. 2009;17:15-22.
62. Qin H, Luo Z, Sun Y, et al. Low-intensity pulsed ultrasound promotes skeletal muscle regeneration via modulating the inflammatory immune microenvironment. *Int J Biol Sci*. 2023;19(4):1123-1145.
63. Huang D, Gao Y, Wang S, et al. Impact of low-intensity pulsed ultrasound on transcription and metabolite compositions in proliferation and functionalization of human adipose-derived mesenchymal stromal cells. *Sci Rep*. 2020;10(1):13690.

64. He R, Zhou W, Zhang Y, et al. Combination of low-intensity pulsed ultrasound and C3H10T1/2 cells promotes bone-defect healing. *Int Orthop*. 2015;39(11):2181-2189.
65. Zhang RL, Zhang ZG, Lu M, Wang Y, Yang JJ, Chopp M. Reduction of the cell cycle length by decreasing G1 phase and cell cycle reentry expand neuronal progenitor cells in the subventricular zone of adult rat after stroke. *J Cereb Blood Flow Metab*. 2006;26(6):857-863.
66. Hulleman E, Boonstra J. Regulation of G1 phase progression by growth factors and the extracellular matrix. *Cell Mol Life Sci*. 2001;58(1):80-93.
67. Zhang RL, Zhang ZG, Roberts C, et al. Lengthening the G(1) phase of neural progenitor cells is concurrent with an increase of symmetric neuron generating division after stroke. *J Cereb Blood Flow Metab*. 2008;28(3):602-611.
68. Yoon S, Seger R. The extracellular signal-regulated kinase: multiple substrates regulate diverse cellular functions. *Growth Factors*. 2006;24(1):21-44.
69. Zuccarini M, Giuliani P, Frinchi M, et al. Uncovering the signaling pathway behind extracellular guanine-induced activation of NO system: new perspectives in memory-related disorders. *Front Pharmacol*. 2018;9:110.
70. Sato M, Nagata K, Kuroda S, et al. Low-intensity pulsed ultrasound activates integrin-mediated mechanotransduction pathway in synovial cells. *Ann Biomed Eng*. 2014;42(10):2156-2163.
71. Gingras AC, Wong CJ. Proteomics approaches to decipher new signaling pathways. *Curr Opin Struct Biol*. 2016;41:128-134.
72. Dakup PP, Feng S, Shi T, Jacobs JM, Wiley HS, Qian WJ. Targeted quantification of protein phosphorylation and its contributions towards mathematical modeling of signaling pathways. *Molecules*. 2023;28(3):1143.
73. Ramanan VK, Shen L, Moore JH, Saykin AJ. Pathway analysis of genomic data: concepts, methods, and prospects for future development. *Trends Genet*. 2012;28(7):323-332.
74. Ochsner SA, Abraham D, Martin K, et al. The signaling pathways project, an integrated 'omics knowledgebase for mammalian cellular signaling pathways. *Sci Data*. 2019;6(1):252.
75. Aliabouzar M, Zhang LG, Sarkar K. Lipid coated microbubbles and low intensity pulsed ultrasound enhance chondrogenesis of human mesenchymal stem cells in 3D printed scaffolds. *Sci Rep*. 2016;6:37728.
76. Osborn J, Aliabouzar M, Zhou X, Rao R, Zhang LG, Sarkar K. Enhanced osteogenic differentiation of human mesenchymal stem cells using microbubbles and low intensity pulsed ultrasound on 3D printed scaffolds. *Adv Biosyst*. 2019;3(2):e1800257.
77. Jin L, Shan J, Hao Y, Wang Y, Liu L. Enhanced bone regeneration by low-intensity pulsed ultrasound and lipid microbubbles on PLGA/TCP 3D-printed scaffolds. *BMC Biotechnol*. 2023;23(1):13.
78. Xu DF, Qu GX, Yan SG, Cai XZ. Microbubble-mediated ultrasound outweighs low-intensity pulsed ultrasound on osteogenesis and neovascularization in a rabbit model of steroid-associated osteonecrosis. *Biomed Res Int*. 2018;2018:4606791.

SUPPORTING INFORMATION

Additional supporting information can be found online in the Supporting Information section at the end of this article.

How to cite this article: Al-Maswary AA, Walmsley AD, Cooper PR, Scheven BA. Low-intensity pulsed ultrasound induces proliferation of human neural stem cells. *Clin Transl Disc*. 2024;4:e259.
https://doi.org/10.1002/ctd2.259